Received 3 February 2005
Revised 9 May 2006
Accepted 30 June 2006

Investigation of heat transfer and pressure drop for various obstacles in a rectangular-sectioned 90° bend

Sebahattin Ünalan, Selahaddin Orhan Akansu and Ahmet Konca
Department of Mechanical Engineering,
Erciyes University Engineering Faculty, Kayseri, Turkey

Abstract

Purpose – $Re < 95{,}000$ based on hydraulic diameter, heat transfer and turbulent flow through a rectangular-sectioned 90° bend was investigated numerically and experimentally. To develop turbulence level, square prism and cylindrical obstacles was placed in the center of the bend.

Design/methodology/approach – For heat transfer, uniform heat flux of 5,000 W/m^2 from bend surfaces is assumed. Numerical analysis was realized for both the turbulent flow and heat transfer. For numerical study, FLUENT 6.1.22 code, RSM turbulence model, hybrid hexahedral-tetrahedral cell structures and uniform inlet velocity assumption were selected. For the pressure distribution in the bend and velocity profile at the outlet of the bend, the experiments was carried out by means of manometers with ethyl alcohol, Mano-air 500 Equipment and pitot-static tube.

Findings – There was a high level of validation obtained between the numerical and the experimental results. Thereby, the mentioned numerical calculation method can be used most engineering applications. For $Re > 20{,}000$, the square prism obstacles provide higher turbulence level and more favorable heat transfer than cylindrical obstacles. For $Re < 20{,}000$, the obstacle use would not require for enhanced heat transfer aim. The obstacle in the bend cause considerably pressure drop in the bend.

Originality/value – The turbulent flow in the bend without obstacle has been numerically investigated by various turbulence models with the non-refined mesh structure and various wall functions. For numerical solution of the turbulence flows and the heat transfer in the rectangular bend with obstacles, the FLUENT code and RSM turbulence model with enhanced wall functions are selected. In order to adapt the cell size and number to the turbulent flow the mesh structure was refined over curvature of turbulence dissipation rate in the bend.

Keywords Heat transfer; Flow, Pressure

Paper type Research paper

Introduction

Developing turbulent flow through 90°-curved bends occurs in several engineering applications such as draft tube of hydraulic turbines, centrifugal pumps, internal combustion engines, gas turbines and air conditioning systems. Accurate prediction of flow field, pressure drop and heat transfer in 90°-curved cooling and heating ducts is of great importance for optimizing the performance of these machines, improving their durability, reducing their fuel consumption, restricting their environmental impact. Generally, the flow in the mentioned applications is turbulent, and the turbulence flow plays an important role over the heat transfer capacity of the systems with forced convection. On the other hand, the geometries for the mentioned systems have highly three-dimensional (3D) and complex characters. The experimental studies would be

International Journal of Numerical Methods for Heat & Fluid Flow
Vol. 17 No. 5, 2007
pp. 494-511

0961-5539
DOI 10.1108/09615530710752964

very difficult, and the validity of experimental results would be limited by complex character, measurement difficulties and accuracy. In addition, time and cost of the experimental studies could not be at a reasonable level. Consequently, detailed information with the best predictions about flow in 90°-curved bends at lowest cost and in acceptable time can be very valuable with the fast improvement of computational fluid dynamics (CFD) software supporting development of higher performance and lower price of computers.

In order to enhance the heat flux, use of turbulators such as baffles, ribs, helical springs and metal rings located in the internal surfaces of the ducts are methods used in the applications. The turbulator increases the heat transfer surface and turbulence level of the flow. This technique used in different applications is a highly preferable method to increase heat transfer coefficient of a fluid with increasing turbulence level. A typical application is the air heating systems with the obstacles. Mochizuki *et al.* (1999) have investigated experimentally local heat transfer coefficients and fluid flow two straight, in turbulent flow through smooth and rib-roughened serpentine passages with a 180° sharp bend. They tested both smooth and ribbed channel walls. In this paper, the increasing heat transfer coefficient with ribbed channel walls was reported. Experimentally, in order to promote turbulence and enhance convective heat transfer, Tanda (2004) investigated the effects of repeated ribs placed to heat exchange surfaces of rectangular channel. The surfaces are heated by uniform heat flux and roughened repeated rid, having rectangular or square sections. According to results of smooth channel without rib, Tanda (2004) indicated that features of the inter-rib distributions of the heat transfer coefficient are strongly related to rib shape and geometry. Wang and Chen (2002) numerically investigated forced convection for flow through a periodic array of a wavy-wall channel. They concluded that the flow through a periodic array of a wavy-wall channel forms a highly complex flow pattern, which comprises a strong forward flow and an oppositely directed re-circulating flow with each wave, that the heat transfer enhancement is not significant at smaller amplitude-wavelength ratio of the periodic array. Lee and Abdel-Moneium (2001) numerically studied heat transfer and flow behaviors past a horizontal surface with 2D transverse ribs. This paper has demonstrated that the presence of transverse ribs yields a significant enhancement of the heat transfer compared with that for a flat plate and the predicted heat transfer coefficients showed good agreement with previous experimental results. ŞŞara (2003) conducted the performance experiments of the rectangular ducts with staggered square pin fins and obtained the average Nusselt number correlation. Hsieh *et al.* (2004) examined the effects of jet impinging positions on heat transfer from rib-roughened (square and semi-circular) channels with rotational speeds of up to 600 rpm. Kondepudi and O'Neal (1991) experimentally studied the effects of frost growth on thermal performance of tube fin heat exchangers with wavy and corrugated fins. The results, contrary previous reports, showed that the energy transfer coefficient was approximately constant throughout the test. In addition, it was indicated that the latent portion of overall energy transfer process was approximately 40 percent of the total. Harris and Goldschmidt (1998) experimentally investigated an empirical investigation into the external heat transfer of a U-bend in cross-flow. Chung *et al.* (2003) numerically investigated unsteady laminar flow and convective heat transfer in a sharp 180° bend. In the paper, the two-dimensionality assumptions are validated by 3D test simulations. Results show that the flow remains steady until Reynolds number (Re) $\approx$ 600. The flow oscillation caused a substantial reduction in the re-attachment length

and a dramatic heat transfer enhancement. The correlation between the flow and the heat transfer is found to be strong. Iacovides *et al.* (2001) studied flow and heat transfer in a rotating U-bend with 45° ribs using CFD methods. They reported that the angled ribs generate stream-wise vortices which, together with the enhanced mixing induced by the ribs, means that the flow and average Nusselt numbers were relatively unaffected by rotation. However, the rotation leaded large temperature gradients in an actual blade. Lee *et al.* (1997) numerically investigated mixed convection heat and mass transfer in a vertical rectangular duct with film evaporation along the porous wall. They concluded that heat transfer along the porous wetted wall is dominated by transport of latent heat in association with the vaporization of water film. Ko and Anand (2003) experimentally investigated average heat transfer coefficient in uniformly heated rectangular channel with wall mounted porous baffles. They obtained that the use of porous baffles resulted in heat transfer enhancement as high as 300 percent compared to heat transfer in straight channel with no baffles. Yang and Hwang (2003) numerically studied on the turbulent fluid flow and heat transfer characteristics for rectangular channel with solid and porous baffles, which are arranged on the bottom and top channel walls in a periodically staggered way. The porous-type baffle channel has a lower friction factor than the solid-type baffle channel. Both the two baffles walls enhanced the heat transfer relative to the smooth channel.

Laminer and turbulent flow through 90°-curved ducts has been extensively studied by many researchers using experimental techniques. The experimental data for a circular curved duct were reported by Enayet *et al.* (1982), Anwer *et al.* (1989) and Sudo *et al.* (1998). These studies collected extensive information about characters of developed flows in curved ducts. Experiments for turbulent flow in a square cross-sectioned 90° bend were realized by Humphrey and Whitelaw (1976), Taylor *et al.* (1982) and Sudo *et al.* (2001). These investigations showed the effects of secondary flow, boundary layer thickness at the start of the bend and inlet velocity profile over the flow development within the squared-sectioned bend. Kim and Patel (1994) studied developing turbulent flow in a 90°-curved duct of rectangular cross-section, and an aspect ratio of 6. They reported that the data provide insights into the development of 3D turbulent boundary layers under the influence of strong stream wise curvature, both convex or concave, and attendant pressure gradients, and clearly elucidate the mechanism by which strong pressure-driven secondary motion results in a longitudinal vortex. In literature, there are a few papers that reported numerical results for turbulent flow through squared and rectangular-sectioned 90° bends. Etemad and Sunden (2006) using four turbulence models investigated numerically the flow and thermal fields in a rectangular-sectioned 90° bend. According to this study, Chen's high-*Re* k-ε model and Suga's cubic low-*Re* k-ε model performed well, while the V2F k-ε model delivered good results and RSM-GGDH model gave poor results. They reported that the boundary layer thickness and the flow upstream of the bend have significant impact on the character of the secondary flow, velocity profile, turbulence level, and heat transfer in the bend. Raisee *et al.* (2006) analyzed turbulent flow in 90°-curved ducts using linear and nonlinear low-*Re* k-ε models. The study showed that the nonlinear k-ε model gives superior predictions of the turbulence field, the pressure and friction coefficients.

In this study, a numerical investigation has been performed to study heat transfer from the bend surfaces to fluid and turbulent flow through a rectangular-sectioned

90° bend. The numerical study extends to determine the effects of square prism and cylindrical obstacles, placed in the center of the bend, in the heat transfer and turbulent flow. In order to clarify validation of numerical results, an experimental study is carried out for measuring of static pressure distribution at the duct surfaces.

Geometry investigation for experimental study and numerical analysis

Figure 1 shows the main dimensions of the rectangular 90°-curved bend geometry selected for numerical and experimental studies. Figure 1(a) shows the perspective of the bend model, measurements points and air inlet-outlet positions, while Figure 1(a) and 1(c) shows the symmetry plane selected for the numerical calculation,

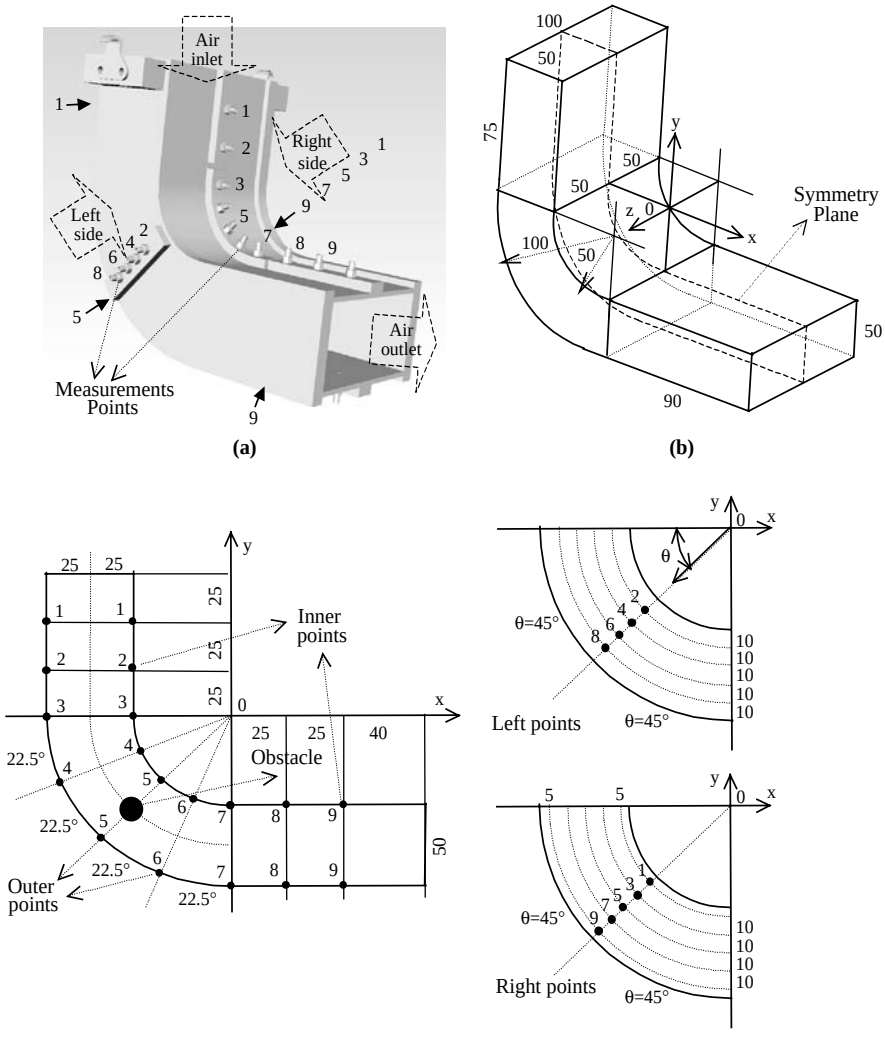

Figure 1.
Illustration of the bend for numerical and experimental studies a) perspective of the model and the measurements points; b) the symmetry plane selected for the numerical calculation, coordinate system and dimensions (mm); c) positions of obstacles and measurements points (mm)

Cartesian Coordinate System and main dimensions in mm, and positions of obstacles and measurements points in mm, respectively. The rectangular section is 5,000 mm^2. The 90°-curved bend height (H) and width ($2H$) are 50 and 100 mm, respectively. The lengths of the duct before and after the curved section are 75 mm ($= 1.5H$) and 90 mm ($1.8H$), respectively. These lengths are considerably lower than those of previous studies. The "y" component of the coordinate system is parallel to gravity vector. The "z" component is perpendicular to sidewalls. The "y" component and "x" component are parallel to the walls of the duct before and after the curved section, respectively. They are perpendicular to inlet and outlet surfaces. Inner and outer radii of the bend are 50 and 100 mm, respectively. The symmetry plane for selected he numerical analysis is surface $z = 0$. Numerical analysis performed for part of the left side-bend to the symmetry plane. Air inlet and outlet directions are $-y$ and $+x$, respectively. The bend inlet is connected to the outlet of a reservoir. The air passed from within the bend exhausts to the atmospheric laboratory medium. The obstacles having square prism and cylindrical geometry are placed into $\theta = 45^{o}$ and a radius of 75 mm of the bend. The selected values for diagonal length (d) of the square prism obstacle and diameter (d) of the cylindrical obstacle are $d = 10$, 15 and 25 mm. For experimental study, the bend shown in Figure 1(a) connected to the air reservoir filled by a fan. The reservoir decreases the turbulence level of air flow after the fan. The air velocity entering to reservoir can be controlled by a tap inserted between the fan and the reservoir. The reservoir out has a decreasing geometry from larger reservoir section to the rectangular section of the bend. The experimental study was performed by three various flow characters: the average inlet velocity, the static pressure distribution and the outlet velocity profile.

For the measurements of the static pressure distribution at the bend surfaces, as seen Figure 1(c), nine points are selected on each one of the inner surface, outer surface and sidewalls of the bend. The pressures differences (ΔP) between the atmospheric medium pressure and the measurements points are measured by means of monometers with ethyl alcohol ($\rho = 0.78\,g/cm^3$). For the bend inlet velocity, ΔP_R ($= P - P_o$) pressure difference between static pressure (P) in the outlet and total pressure (P_o) at the middle of the reservoir is measured by means of monometers with ethyl alcohol. The ΔP_R is the dynamic pressure of the bend inlet or the reservoir outlet. The averaged inlet velocity (U_{avg}) as a function of the ΔP_R measured in Pascal (Pa) can be calculated from following equation combined with ideal gas law:

$$U_{avg} = \sqrt{\frac{2\Delta P_R}{\rho_{air}}} = \sqrt{\frac{2\Delta P_R}{(P_{atm}/RT)}} = \sqrt{\frac{2RT\Delta P_R}{P_{atm}}} \tag{1}$$

Where, R and ρ_{air} are gas constant and air density, respectively. The ρ_{air} is 1.04 kg/m^3, corresponding to the laboratory medium pressure of $P_{atm} = 88$ kPa and the medium temperature of 295 K ($= 22^{o}C$) with ideal gas laws. In addition, validation of the U_{avg} values from ΔP_R measurement and equation (1) is controlled by means of the digital velocity measurements performed by Mano air 500 Equipment and pitot-static tube. In numerical analysis, the calculated U_{avg} is assumed as averaged velocity (uniform inlet velocity) instead of real velocity profile for inlet velocity condition. The pressure distribution experiments without the obstacles are carried out for three velocity values, $U_{avg} = 6.75$ m/s, 10 m/s and 19.04 m/s. For velocity profile measurements at the bend

outlet of the bend without the obstacle and with the cylindrical obstacle of $d = 15$ mm, the average inlet velocity are calculated as $U_{avg} = 17.5$ m/s. The temperature and the pressure of laboratory medium are measured by various thermometers and the aneroid-type barometer, respectively.

The measurement errors were estimate to be $\pm 5\,Pa$ for the manometer and $\pm 1\,K$ for the thermometer. Sensitivity of the manometer indicator and transient variations occurring at free surface of the manometer's liquid causes high errors in the ΔP measurements. This measurement error would be important for low U_{avg} velocities and low ΔP values, especially. The atmospheric pressure measured was assumed as a value faultless value because of checking of the pressure value validation with various methods and literature information. According to estimation method of Kline and McClintock (quoted in Holman (1989)), the uncertainty values in U_{avg} uniform velocity or Reynolds number are found 6.7 and 1.5 percent for $U_{avg} = 6.75$ and 19.04, respectively. On the other hand, geometrical mistakes of the ducts and the position errors of measurement points at the ducts such as axis eccentric, shorter and longer sizes, non-exact circle geometry, etc. must be added to the values. Consequently, the maximum uncertainty may be assumed as ≈ 10 percent, for low U_{avg} velocities especially.

Governing equations

All the flow and energy equations used in the numerical analysis are presented in Cartesian tensor notation in the following sections.

Main flow and energy equations

For a steady compressible flow, the conservation laws of mass, momentum and energy are written as:

$$\text{Continuity;} \quad \frac{\partial(\rho U_j)}{\partial x_j} = 0 \tag{2}$$

$$\text{Momentum;} \quad \frac{\partial(\rho U_j U_i)}{\partial x_j} = -\frac{\partial P}{\partial x_i} + \frac{\partial}{\partial x_j}\left(\mu \frac{\partial U_i}{\partial x_j} - (\rho \overline{u_i u_j})\right) \tag{3}$$

where, P is the pressure, upper and lower case U's denote mean (time-averaged) and fluctuating velocities, and $\rho \overline{u_i u_j}$ is the unknown Reynolds stress.

$$\text{Energy;} \quad \frac{\partial}{\partial x_j}[U_j(\rho E + P)] = \frac{\partial}{\partial x_j}\left(k_{\text{eff}} \frac{\partial T}{\partial x_j} - \sum_j h_j J_j + \frac{\partial}{\partial x_j}\left(\mu U_i \frac{\partial U_j}{\partial x_j}\right)\right) \tag{4}$$

where, k_{eff} and h are the effective conductivity and sensible enthalpy, respectively. J_j is the diffusion flux of species j. In equation:

$$E = h - \frac{P}{\rho} + \frac{U^2}{2} \tag{5}$$

In the calculation, the three terms on the right-hand side of equation (4) represent energy transfer due to conduction, species diffusion and viscous dissipation, respectively.

Turbulence modeling equations and numerical aspects

Numerical solutions of the differential equations given the conservation laws of mass, momentum and energy have been solved using the finite volume code FLUENT (2001). For the mentioned velocities in the previous section, local Reynolds number around the obstacle is well above 450. Thereby, the flow analysis was performed for 3D geometry because of the secondary flow effects in the flow turbulence and the forced convection. The Reynolds stress model (RSM) is selected as the turbulence model in the FLUENT code. The RSM is the most elaborate turbulence model that FLUENT provides. Abandoning the isotropic eddy-viscosity hypothesis, the RSM closes the Reynolds-averaged Navier-Stokes equations by solving transport equations for the Reynolds stresses, together with an equation for the dissipation rate. This means that seven additional transport equations are required in (3D) flows.

Since, the RSM accounts for the effects of streamline curvature, swirl, rotation, and rapid changes in strain rate in a more rigorous manner than one-equation and two-equation models, it has greater potential to give accurate predictions for complex flows. However, the fidelity of RSM predictions is still limited by the closure assumptions employed to model various terms in the exact transport equations for the Reynolds stresses. The modeling of the pressure-strain and dissipation-rate terms is particularly challenging, and often considered to be responsible for compromising the accuracy of RSM predictions.

The RSM might not always yield results that are clearly superior to the simpler models in all classes of flows to warrant the additional computational expense. However, use of the RSM is a must when the flow features of interest are the result of anisotropy in the Reynolds stresses. Among the examples are cyclone flows, highly swirling flows in combustors, rotating flow passages, and the stress-induced secondary flows in ducts (FLUENT, 2001).

The steady transport equations for the transport of the Reynolds stresses solved by the RSM, $-\rho\overline{u_i u_j}$, may be written as follows:

$$\frac{\partial}{\partial x_k}(U_k\rho\overline{u_i u_j}) = -\frac{\partial}{\partial x_k}\left[(\rho\overline{u_i u_j u_k}) + \overline{p(\delta_{kj}u_i + \delta_{ik}u_j)}\right] + \frac{\partial}{\partial x_k}\left(\mu\frac{\partial}{\partial x_k}(\overline{u_i u_j})\right) - \rho\left((\overline{u_i u_j})\frac{\partial U_j}{\partial x_k} + (\overline{u_j u_k})\frac{\partial U_i}{\partial x_k}\right) + \overline{p\left(\frac{\partial u_i}{\partial x_j} + \frac{\partial u_j}{\partial x_i}\right)} - 2\mu\overline{\frac{\partial u_i}{\partial x_k}\frac{\partial u_j}{\partial x_k}} \tag{6}$$

Terms in equation (6) explain convection (C_{ij}), turbulent diffusion ($D_{T,ij}$), molecular diffusion ($D_{L,ij}$), stress production (P_{ij}), pressure strain (ϕ_{ij}) and dissipation (ε_{ij}), respectively. The buoyancy production, production by system rotation and user-defined source terms are not considered in equation (6). The FLUENT uses a scalar turbulent diffusivity as follows:

$$D_{T,ij} = \frac{\partial}{\partial x_k}\left(\frac{\mu_t}{\sigma_k}\frac{\partial}{\partial x_k}(\overline{u_i u_j})\right) \tag{7}$$

Where, σ_k is 0.82.The turbulent viscosity, μ_t, is computed using following equation:

$$\mu_t = \rho C_\mu \frac{k^2}{\varepsilon} \tag{8}$$

In the above equation, k and ε are the turbulence kinetic energy and the turbulence dissipation rate, respectively. C_μ is 0.09. The pressure-strain term (ϕ_{ij}) can be explained by linear pressure-strain model as follows:

$$\phi_{ij} = -C_1\rho\frac{\varepsilon}{k}\left[\overline{u_iu_j} - \frac{2}{3}\,\delta_{ij}k\right] - C_2\left[P_{ij} - C_{ij} - \frac{\delta_{ij}}{3}(P_{kk} - C_{kk})\right] + \phi_{ij,w} \tag{9}$$

$$\begin{aligned}\phi_{ij,w} = {} & C_1^t\frac{\varepsilon}{k}\left(\overline{u_ku_m}n_kn_m\delta_{ij} - \frac{3}{2}(\overline{u_iu_k}n_jn_k + \overline{u_ju_k}n_in_k)\right)\frac{0.4187k^{3/2}}{C_\mu^{3/4}\varepsilon d} \\ & + C_2^t\left(\phi_{km,2}n_kn_m\delta_{ij} - \frac{3}{2}(\phi_{ik,2}n_jn_k + \phi_{jk,2}n_in_k)\right)\frac{0.4187k^{3/2}}{C_\mu^{3/4}\varepsilon d}\end{aligned} \tag{10}$$

Where $C_1 = 1.8, C_2 = 0.6, C_1^t = 0.5, C_2^t = 0.3$, $\phi_{ij,w}$ is the wall-reflection term which is responsible for the redistribution of normal stress near the wall, n_k is the x_k component of the unit normal to the wall, and d is the normal distance to the wall. Enhanced wall treatment is near – wall modeling method that combines a two-layer model with enhanced wall functions. In FLUENT's near wall model, the viscosity-affected near wall region is completely resolved all the way to the viscous sub-layer. The two layer approach is an integral part of the enhanced wall treatment. When the RSM is applied to near – wall flows using the enhanced wall treatment, the pressure-strain model needs to be modified in term of C constants above. The modifications are as follows:

$$\begin{aligned}& C_1 = 1 + 2.58A_1\sqrt{A_2}\left[1 - e^{-(0.0067Re_t)^2}\right], \quad C_2 = 0.75\sqrt{A_3}, \\ & C_1^t = -\frac{2}{3}\,C_1 + 1.67, \quad C_2^t = \max\left(\frac{(2/3)C_2 - (1/6)}{C_2}, 0\right), \\ & A_1 = 1 - \frac{9}{8}(A_2 - A_3), \quad A_2 = a_{ik}a_{ki}, \quad A_3 = a_{ik}a_{kj}a_{ji}\end{aligned} \tag{11}$$

where Re_t defines the turbulent Reynolds number ($= \rho k^2/\mu\varepsilon$). The a_{ij} is the Reynolds – stress anisotropy tensor, as defined:

$$a_{ij} = -\frac{-\rho\overline{u_iu_j} + (2/3)\rho k\delta_{ij}}{\rho k} \tag{12}$$

The turbulence kinetic energy ($k = (1/2)\overline{u_iu_i}$) and its scalar dissipation rate (ε) are obtained from the following transport equations:

$$\frac{\partial}{\partial x_i}(\rho kU_i) = \frac{\partial}{\partial x_j}\left(\left(\mu + \frac{\mu_t}{0.82}\right)\frac{\partial k}{\partial x_j}\right) + \frac{1}{2}\,P_{ii} - \rho\varepsilon(1 + 2\mu_t^2) \tag{13}$$

$$\frac{\partial}{\partial x_i}(\rho\varepsilon U_i) = \frac{\partial}{\partial x_j}\left(\left(\mu + \frac{\mu_t}{1.0}\right)\frac{\partial k}{\partial x_j}\right) + \frac{1.44}{2}\,\frac{\varepsilon}{k}\,P_{ii} - 1.92\rho\frac{\varepsilon^2}{k} \tag{14}$$

The dissipation tensor is modeled by $\varepsilon ij = (2/3)\delta_{ij}\rho\varepsilon(1 + 2(k/\gamma RT))$ for the compressible form of the ideal gas. With the Reynolds stress model in FLUENT,

turbulent heat transport is modeled using the concept of Reynolds' analogy to turbulent momentum transfer. The modeled energy equation is the given by the following:

$$\frac{\partial}{\partial x_i}(U_i(\rho E + p)) = \frac{\partial}{\partial x_j}\left(\left(k + \frac{C_p \mu_t}{Pr_t}\right)\frac{\partial T}{\partial x_j} + U_i \mu_{\text{eff}}\left(\frac{\partial U_j}{\partial x_i} + \frac{\partial U_i}{\partial x_j} - \frac{2}{3}\frac{\partial U_i}{\partial x_i}\delta_{ij}\right)\right) \quad (15)$$

where the turbulent Prandtl number, Pr_t, is 0.85. δ_{ij} is Kronecker δ. Equation (15) includes the viscous heating term. Whenever flow enters the domain, FLUENT requires values for individual Reynolds stresses, $\rho\overline{u_i u_j}$, and for the turbulence dissipation rate, ε. These quantities can be input directly or derived from the turbulence intensity and characteristic length. At walls, FLUENT computes the near-wall values of the Reynolds stresses and ε from wall functions. FLUENT applies explicit wall boundary conditions for the Reynolds stresses by using the log-law and the assumption of equilibrium, with disregarding convection and diffusion in the transport equations for the stresses. Using a local coordinate system, where τ is the tangential coordinate, η is the normal coordinate, and λ is the bi-normal coordinate, the Reynolds stresses at the wall-adjacent cells are computed from:

$$\frac{\overline{u_\tau^2}}{k} = 1.098, \quad \frac{\overline{u_\eta^2}}{k} = 0.247, \quad \frac{\overline{u_\lambda^2}}{k} = 0.655, \quad -\frac{\overline{u_\eta u_\tau}}{k} = 0.255 \quad (16)$$

To obtain k, FLUENT solves the transport equation of equation (13). In the numerical calculations, boundary condition types of the inlet and outlet are selected as "inlet velocity = uniform U_{avg} velocity" and "pressure outlet = the atmospheric medium" from FLUENT panel. In the inlet and outlet of the bend, the turbulence specification method and Reynolds-stress specification method are selected as k-ε and k-or-turbulence intensity, respectively. The k and ε values for inlet and outlet of the duct are estimated from following equations:

$$I = 0.16(\text{Re}_D)^{-1/8}, \quad \ell = 0.07 D_H, \quad k = \frac{3}{2}(IU_{\text{avg}})^2, \quad \varepsilon = C_\mu^{3/4}\frac{k^{3/2}}{\ell} \quad (17)$$

Where Re_{D} is the Reynolds number, based on the hydraulic diameter (D_{H}). I and l are the turbulence intensity and the turbulence length scale, respectively. For thermal calculations, inlet temperature of the air is 295 K. All surfaces of the bend were heated by a uniform heat flux (q'') of 5,000 W/m^2, except the surfaces of the obstacles. Numeric calculations were realized for uniform inlet velocities of $U_{\text{avg}} = 5$, 10, 15, 20 and 25 m/s. The density (ρ) of the air is calculated by the ideal gas approach. In addition, thermal conductivity (k_{eff}), specific heat (C_{p}), and dynamic viscosity (μ) of the air are considered as a function of the flow temperature. These functions can be explained by means of a fourth degrees polynomial, analytically. The constant of these equations are given in Table I. The required data are taken from (Cengel, 1997).

As shown in Figure 1(b), due to symmetry in the curved rectangular bend and in the flow conditions, only half of the cross-section is resolved using a mesh, and symmetry-plane condition was applied. The origin of the coordinate system corresponds on the center of curvature. In the references Etemad and Sunden (2006) and Raisee *et al.* (2006), the rectangular prism mesh structure has been preferred. In the numerical solutions, the shape of the cell (including its skewness and aspect ratio) also has a significant impact on the accuracy on the results. The cell structure

	A	B	C	D	E
k_{eff} [W/mK]	2.064614×10^{-03}	8.731414×10^{-05}	$-2.641003 \times 10^{-08}$	4.008917×10^{-12}	0
C_p [J/kgK]	$1.033094 \times 10^{+03}$	$-2.989620 \times 10^{-01}$	8.350206×10^{-04}	$-5.536863 \times 10^{-07}$	1.239482×10^{-10}
[a] μ [Kg/ms]	1.660072×10^{-06}	6.693351×10^{-08}	$-4.120350 \times 10^{-11}$	1.728613×10^{-14}	$-2.921590 \times 10^{-18}$

Note: [a] $\mu(T) = A + BT + CT^2 + DT^3 + ET^4$

Table I.
Constant values for equations of λ C_p, and μ as function of temperature

has to correspond to physical character of the gas flow or liquid flow. Thereby, the hybrid mesh structures made of the hexahedral and tetrahedral geometries are preferred for the rectangular bend with obstacles. To establish grid independency, extensive grid studies were carried out. The grid densities in the bend were varied for interval sizes between 1 and 3 mm until the grid independency was obtained. Also, the impact of the y^+ value (<1) for the wall-adjacent cells on the results was explored. Therefore, the reached cell numbers are about 700,000. In addition, after the numerical iteration reached to the convergence criteria of 0.0001, in order to adapt the cell size and number to the turbulent flow, the mesh structure was refined over curvature of turbulence dissipation rate (ε) in the bend. The numerical calculations were repeated with new mesh structure. The refinement process was performed five times for the bend with square prism of 25 mm, in particularly. Consequently, the cell numbers increased up to $\approx$ two million. For obstacles of 25 mm, the final mesh structures in the symmetry plane can be shown in Figure 2. As seen in the figure, the cell sizes increase from the obstacle surfaces towards the flow medium.

Results

This paper investigated the heat transfer with the forced convection and the effects of the turbulent flow through a rectangular-sectioned 90° bend on the pressure drop. The turbulent flow and heat transfer was modeled numerically, while only the pressure drop in the bend investigated experimentally and numerically. The experiments would obtain the validation of the numerical results. The turbulent flow plays an important role on the pressure drop and the heat transfer with forced convection. Thereby, the high correlation between the numerical results and the experiments for the pressure drop would validate results obtained for heat transfer in terms of real applications. At this point, the other micro flow characteristics such as pressure distribution, vortices, velocity profile in the bend could also be considered. However, in the application, researchers and engineers who are interested in the flow through the bend and pipeline need macro information such as the pressure drop coefficient and the convection heat transfer coefficient. On the other hand, the mentioned flow characteristics have been extensively investigated by previous studies (Etemad and Sunden, 2006; Raisee *et al.*, 2006). The main aim in this paper is to demonstrate that the parameters mentioned above can be calculated by means of a CFD code within acceptable limits of error.

For four cases, $Re = 26{,}350$ (a), $Re = 38{,}940$ (b), $Re = 74{,}140$ (c) without the obstacles and $Re = 68{,}150$ with the cylindrical obstacle of $d = 15$ mm, Figure 3 shows numerical and experimental pressure differences (ΔP) in the 27 measurement points in the inner (convex), outer (concave) and sidewalls (radial) seen in Figure 1. Figure would give the information about pressure distribution of the bend surfaces. As expected, due to the action of the centrifugal force, variation of the pressure difference showed two various characters along the convex side and the concave side from the inlet to the outlet. At the midpoint of the bend without obstacles ($\theta = 45^{o}$, point number:5), the ΔP curve has a minimum point (vacuum pressure) for the convex side, while the ΔP curve has a maximum point for the concave side. The minimum and maximum ΔP values increased with Re number. The values are -18 Pa and 19 Pa for $Re = 26{,}350$, -180 Pa and 110 Pa for $Re = 74{,}140$. In addition, the ΔP values for sidewalls (radial) increased from inner side to outer side corresponding to that of the behavior at the $\theta = 45^{o}$. The ΔP curve of concave side of the bend with cylindrical obstacle shows different behavior.

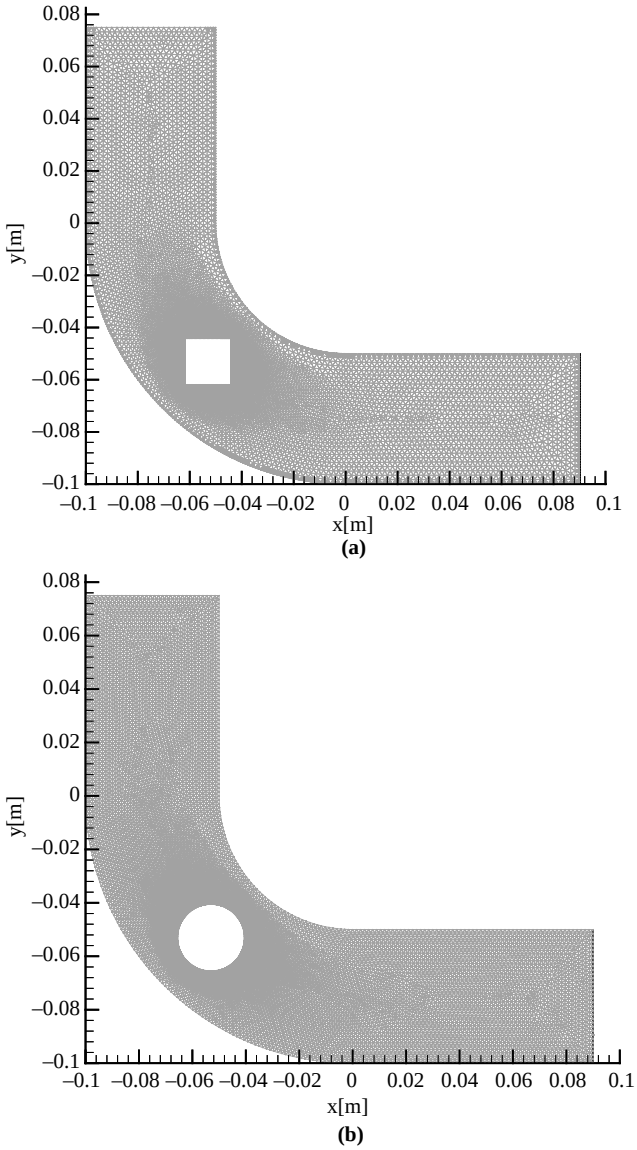

Figure 2.
A view of the last mesh structures for the square and cylindrical obstacles of $d = 25$ mm at the symmetry plane

The curve has two maximum points, at point 4 and point 6. However, the cylindrical obstacle does not quite affect the main character of the pressure distribution along the convex side of the bend. The minimum pressure ($-220\,Pa$ for $Re = 68{,}150$) is higher than in the case without the obstacle ($-180\,Pa$ for $Re = 74{,}140$). The main conclusion from Figure 3 is high validation obtained between the numerical and the experimental results. These results can be accepted as far as many engineering applications are concerned, though the manometer measurement error of ± 5 Pa, uniform velocity

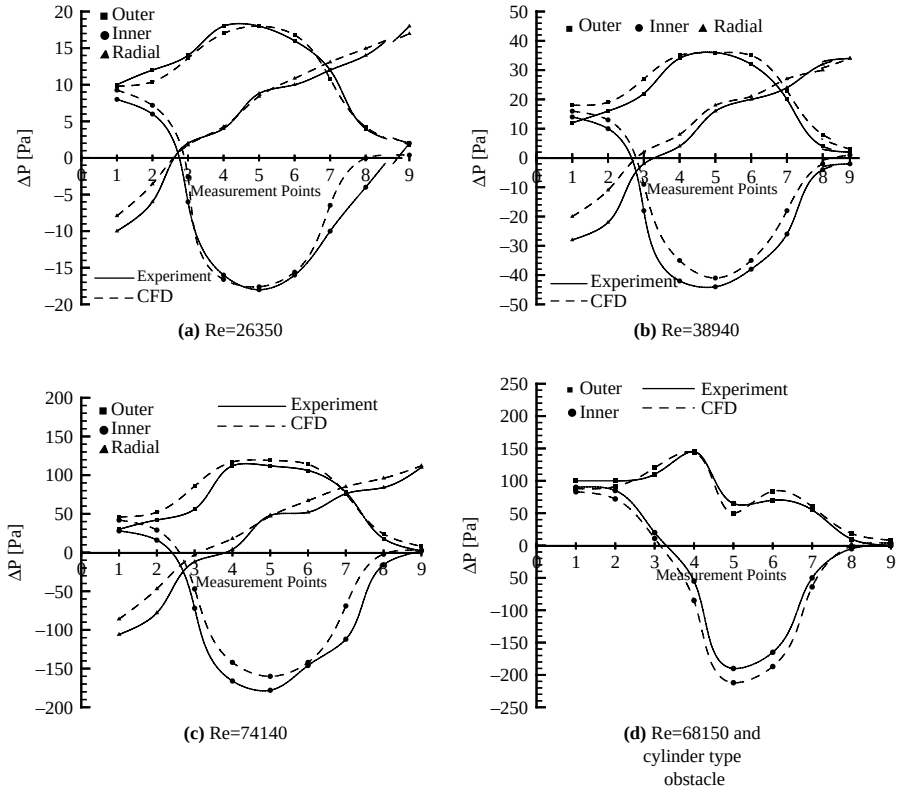

Figure 3.
Numerical and experimental pressure differences for various Reynolds number and cases

assumption in the inlet and the uncertainty of Reynolds number ≈ 10 percent. Figure 4 shows contours of the velocity magnitudes (a) and secondary flow vectors (b) on the outlet surface of the bend for flows without the obstacles. The maximum values of the velocity magnitudes occurred in region close to outer surface. The bend curvature induces counter-rotating secondary vortices at the region close inner surface and sidewall. These results are close to those of previously studies (Sudo *et al.*, 2001; Kim and Patel, 1994; Etemad and Sunden, 2006; Raisee *et al.*, 2006). For cases with the cylindrical obstacle of $d = 15$ mm and without obstacle having inlet velocity of 17.5 m/s, Figure 5 shows the measured and calculated longitudinal mean velocity ($\times$ component of velocity magnitude) profile (a) and the calculated secondary flow vectors (b) on the outlet surface of the investigated bend. In the Figure 5(a), W is ratio to uniform inlet velocity of 17.5 m/s of longitudinal mean velocity in m/s. Figure 5(a) indicates good validation for case without obstacle and poor validation for case with obstacle between the measurements and calculations. Especially, it obtained important difference between the calculated and measured values velocities at outer side of the bend outlet with obstacle. In addition, the used measurement equipment exhibited poor performance in the measurement of boundary layer effects in the regions close to the walls. However, the obtained results indicate that the method used in numerical calculation is reliable in

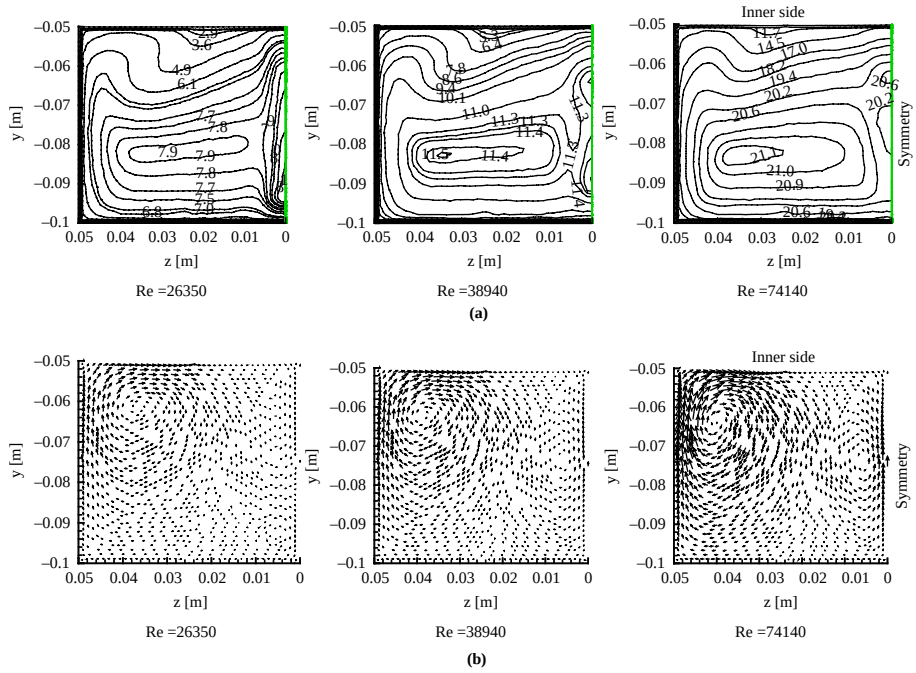

Figure 4.
Counters of velocity magnitude and secondary flow velocity vectors on the outlet of the bend for various Reynolds number

terms of macro engineering analyses. According to numerical result from Figure 5(b), the obstacle causes many secondary flows on the outlet surface. As expected, this shows increased turbulence level in the bend with obstacle. Consequently, Figures 1-5 prove that the used numerical elementary type, the RSM turbulence model and FLUENT CFD code, would be a calculation method to be preferred for turbulent flow through a rectangular-sectioned 90° bend. On the contrary to reference Etemad and Sunden (2006), the RSM is an acceptable turbulence model for prediction of turbulent flow in the bend. At this point, it must be borne in mind again that the shape of the cell (including its skewness and aspect ratio) has a significant impact on the accuracy of the numerical results, and the mesh structure is refined by the adapting process corresponding to the flow character. Therefore, also the numerical results obtained through the same calculation method for the bend with various obstacles would be valid. The acceptable heat transfer analysis would be possible with real prediction of the turbulence flow. Figures 6 and 7 show variation of Nusselt number and the pressure coefficient versus Reynolds number for the investigated all cases, respectively. Nusselt number (Nu), Reynolds number (Re) and pressure coefficient (C_{pf}) are calculated as follows:

$$h = \frac{q''}{T_{\text{wall}} - T_{\text{bulk}}} \tag{18}$$

$$Nu = \frac{h D_{\text{H}}}{k} \tag{19}$$

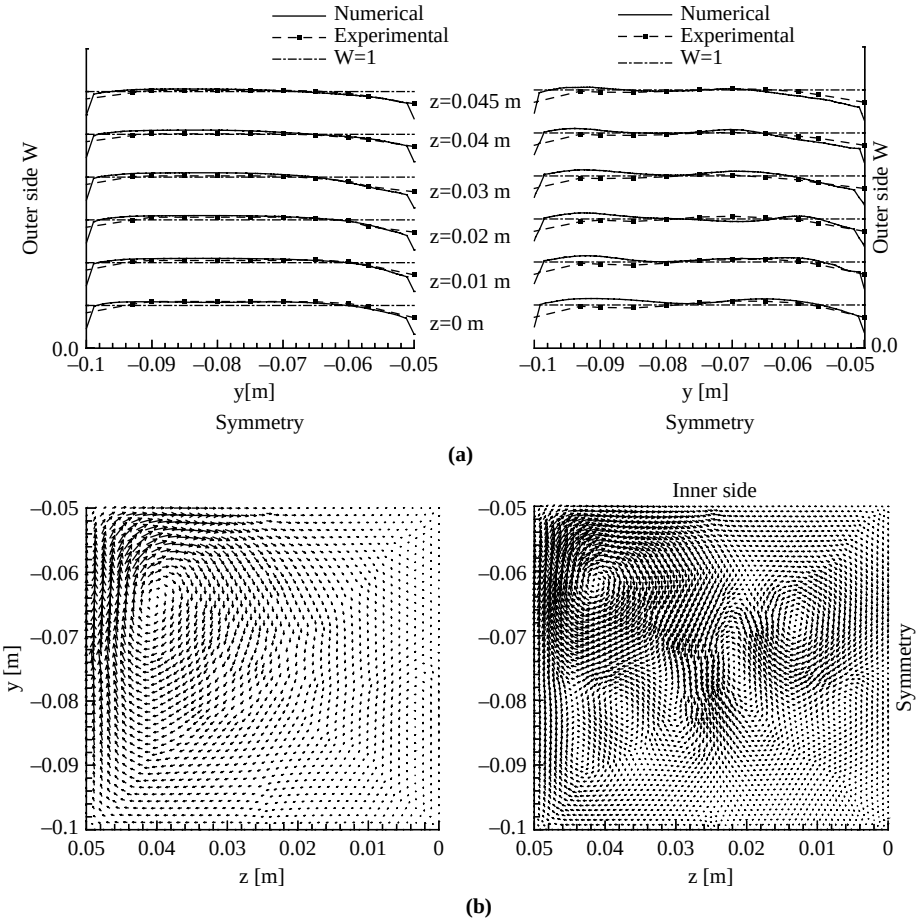

Figure 5.
The velocity profile on the outlet surface (a) and secondary velocity vectors (b) for cases without obstacle (left) and cylindrical obstacles of 15 mm (right)

$$Re = \frac{\rho U_{\text{avg}} D_{\text{H}}}{\mu} \tag{20}$$

$$C_{\text{pf}} = \frac{\Delta P_{\text{b}}}{((1/2)\rho U_{\text{avg}}^2)} \tag{21}$$

Where; ΔP_{b}, μ, T_{bulk} and T_{wall} are pressure drop between inlet and outlet of the bend, dynamic viscosity of air, bulk and wall surface temperatures, respectively. For curves in Figures 6 and 7, ΔP_{b} and T_{wall} are averaged by means of area-weighted-integral, while ρ, μ, k and T_{bulk} are averaged by means of mass-weighted-integral.

According to Figure 6, as expected, Nusselt number improved with increasing of d, which is diagonal length of the square prism obstacles and diameter of the cylindrical obstacles. Cylindrical obstacles cause less improvement than those of square prism obstacle. For cylindrical obstacles of $d = 10$ and 15 mm, improvement of Nusselt

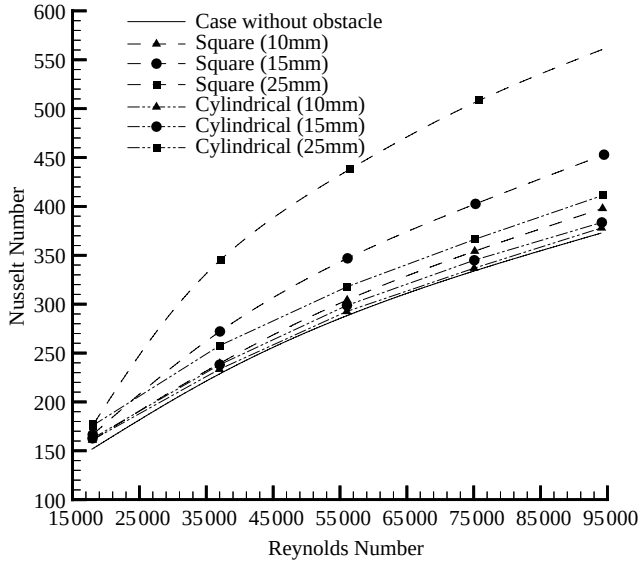

Figure 6.
Nusselt numbers versus Reynolds number for various cases

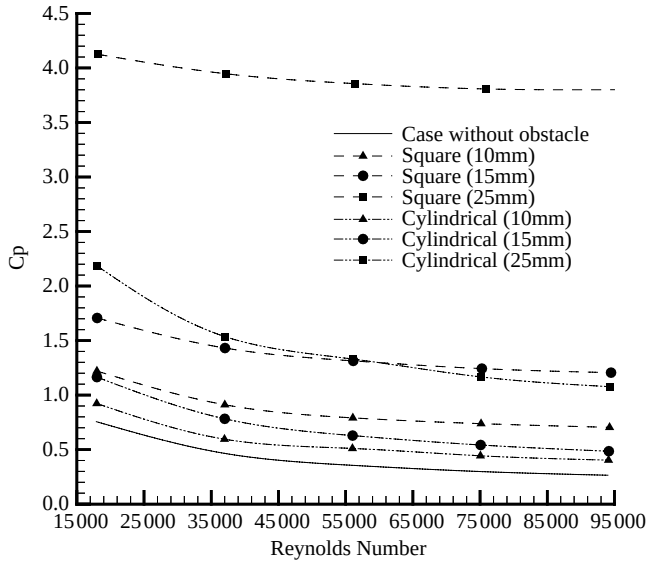

Figure 7.
Pressure coefficient of the bend versus Reynolds numbers

number can be ignored. For $Re < 20{,}000$, neither obstacles yielded good performance. In these cases, the turbulence developing around the obstacles cannot reach wall surfaces. On the other hand, sharp edges of square prism obstacles considerably increased the turbulence level of the flow in the bend. Therefore, the square prism obstacles would be preferred for their high heat transfer capability from wall surfaces to fluid. However, Figure 7 shows that square obstacles cause higher pressure drop

between the inlet and outlet on the bend. For high *Re* numbers and square obstacle of $d = 25$ mm, the heat transfer improved by 50 percent, while the pressure drop increased 8 times.

Conclusions

In this study, heat transfer from the bend surfaces to fluid and turbulent flow through a rectangular-sectioned 90° bend was investigated numerically and experimentally. In order to develop turbulence level, square prism and cylindrical obstacles were placed in the center of the bend. For heat transfer, uniform heat flux of 5,000 W/m^2 from bend surfaces is assumed. Numerical analysis realized for both the turbulent flow and heat transfer. For numerical study, FLUENT code, RSM turbulence model, hybrid hexahedral-tetrahedral mesh structures and uniform inlet velocity assumption are preferred. In order to adapt the cell size and number to the turbulent flow, the mesh structure was refined over curvature of turbulence dissipation rate in the bend. For the pressure distribution in the bend and velocity profile on the outlet surface of the bend, the experimental study is carried out by means of manometers with ethyl alcohol, Mano air 500 Equipment and pitot – static tube. Conclusions can be summarized as follows:

- There is high validation obtained between the numerical and the experimental results. Thereby, the above mentioned numerical calculation method can be used in most engineering applications in the turbulent flow.
- The square prism obstacles provide higher turbulence level and improved heat transfer compared to cylindrical obstacles. For low *Re*, the obstacle use would not require for enhanced heat transfer aim.
- The obstacle in the bend cause considerable pressure drop in the bend.

References

Anwer, M., So, R.M.C. and Lai, Y.C. (1989), "Perturbation by and recovery from bend curvature of a fully-developed turbulent flow", *Physics Fluids*, Vol. 1 No. 8, pp. 1387-97.

Cengel, Y. (1997), *Heat Transfer: A Practical Approach*, McGraw-Hill, Boston, MA.

Chung, Y.M., Tucker, P.G. and Roychowdhury, D.G. (2003), "Unsteady laminar flow and convective heat transfer in a sharp 180° bend", *International Journal of Heat and Fluid Flow*, Vol. 24 No. 1, pp. 67-76.

Enayet, M.M., Gibson, M.M., Taylor, A.M.K.P. and Yianneskis, M. (1982), "Laser-Doppler measurements of laminer and turbulent flow in a pipe bend", *International Journal of Heat and Fluid Flow*, Vol. 3, pp. 213-9.

Etemad, S. and Sunden, B. (2006), "Numerical investigation of turbulent heat transfer in a rectangular-sectioned 90° bend", *Numerical Heat Transfer, Part A*, Vol. 49, pp. 323-43.

FLUENT 6.1.22 (2001), *User's Guide Fluent Incorporated*, NH. 03766, Lebanon.

Harris, D.K. and Goldschmidt, V.W. (1998), "An empirical investigation into the external heat transfer of a U-bend in cross-flow", *International Journal of Heat and Mass Transfer*, Vol. 42 No. 11, pp. 1957-68.

Holman, J.P. (1989), *Experimental Methods for Engineers*, McGraw-Hill, New York, NY.

Hsieh, S-S., Tsai, H-H. and Chan, S-C. (2004), "Local heat transfer in rotating square-rib-roughened and smooth channels with jet impingement", *International Journal of Heat Mass Transfer*, Vol. 47, pp. 229-43.

Humphrey, J.A.C. and Whitelaw, J.H. (1976), "Measurements in curved flows", *Proceedings of the SQUID Conference Internal Flows, Airlie House*.

Iacovides, H., Jackson, D.C., Kelemenis, G., Launder, B.E. and Yuan, Y.M. (2001), "Flow and heat transfer in a rotating U-bend with 45° ribs", *International Journal of Heat and Fluid Flow*, Vol. 22 No. 3, pp. 308-14.

Kim, W.J. and Patel, V.C. (1994), "Origin and decay of longitudinal vortices in developing flow in a curved rectangular duct", *Journal of Fluids Engineering*, Vol. 116, pp. 45-52.

Ko, K-H. and Anand, N.K. (2003), "Use of porous baffles to enhance heat transfer in a rectangular channel", *International Journal of Heat and Mass Transfer*, Vol. 46, pp. 4191-9.

Kondepudi, S.N. and O'Neal, D.L. (1991), "Frosting performance of tube fin heat exchangers with wavy and corrugated fins", *Experimental Thermal& Fluid Science*, Vol. 4, pp. 613-8.

Lee, C.K. and Abdel-Moneium, S.A. (2001), "Computational analysis of heat transfer in turbulent flow past a horizontal surface with two-dimensional ribs", *International Communications in Heat and Mass Transfer*, Vol. 28 No. 2, pp. 161-70.

Lee, K-T., Tsai, H-L. and Yan, W-M. (1997), "Mixed convection heat and mass transfer in vertical rectangular ducts", *International Journal of Heat and Mass Transfer*, Vol. 40, pp. 1621-31.

Mochizuki, S., Murata, A., Shibata, R. and Yang, W-J. (1999), "Detailed measurements of local heat transfer coefficients in turbulent flow through smooth and rib-roughened serpentine passages with a 180° sharp bend", *International Journal of Heat and Mass Transfer*, Vol. 42, pp. 1925-42.

Raisee, M., Alemi, H. and Iacovides, H. (2006), "Prediction of developing turbulent flow in 90°-curved ducts using linear and non-linear low-Re k-ε models", *International Journal for Numerical Methods in Fluids*, Vol. 51 No. 12, pp. 1379-405.

Şara, O.N. (2003), "Performance analysis of rectangular ducts with staggered square pin fins", *Energy Conversion & Management*, Vol. 44, pp. 1787-803.

Sudo, K., Sumida, M. and Hibara, H. (1998), "Experimental investigation on turbulent flow through a circular-sectioned 90° bend", *Experiments in Fluids*, Vol. 25, pp. 42-9.

Sudo, K., Sumida, M. and Hibara, H. (2001), "Experimental investigation on turbulent flow in a square-sectioned 90° bend", *Experiments in Fluids*, Vol. 30, pp. 246-52.

Tanda, G. (2004), "Heat transfer in rectangular channels with traverse and V-shaped broken ribs", *International Journal of Heat and Mass Transfer*, Vol. 47, pp. 229-43.

Taylor, A.M.K.P., Whitelaw, J.H. and Yianneskis, M. (1982), "Curved ducts with strong secondary motion: velocity measurements of developing laminar and turbulent flows", *Journal of Fluids Engineering*, Vol. 104, pp. 350-9.

Wang, C-C. and Chen, K. (2002), "Forced convection in a wavy-wall channel", *International Journal of Heat and Mass Transfer*, Vol. 45, pp. 2587-95.

Yang, Y-T. and Hwang, C-Z. (2003), "Calculation of turbulent flow and heat transfer in a porous-baffled channel", *International Journal of Heat and Mass Transfer*, Vol. 46, pp. 771-80.

Corresponding author
Selahaddin Orhan Akansu can be contacted at: akansu@erciyes.edu.tr